Chow, Y. C., & McGeehan, J. P. (2004). Error-bound formulation for multichannel reception of M-DPSK and pilot-aided M-PSK over Rayleigh-fading channels with postdetection combining. IEEE Transactions on Vehicular Technology, 53(3), 747 - 757. 10.1109/TVT.2004.827160

Error-Bound Formulation for Multichannel Reception of M-DPSK and Pilot-Aided M-PSK Over Rayleigh-Fading Channels With Postdetection Combining

Yuk C. Chow, *Associate Member, IEEE,* and Joe P. McGeehan

***Abstract*—Upper bounds for symbol-error probability are developed for multichannel reception of M-ary phase-shift keying (M-PSK) over frequency-flat Rayleigh-fading channels. Differential coherent demodulation of differentially encoded M-PSK (M-DPSK), pilot-tone aided coherent demodulation of M-PSK (PTA M-CPSK) and pilot-symbol aided coherent demodulation of M-PSK (PSA M-CPSK) are considered in the formulation. The bounds enable the investigation of the effects of fading correlation and unequal average power level between channels using postdetection diversity reception with maximal-ratio combining. Error-performance degradation due to imperfect demodulation effects, such as Doppler spread in M-DPSK schemes, noisy reference signals in PTA M-CPSK, and PSA M-CPSK schemes can be taken into account in the formulation. Exact bit-error probabilities for both binary and quaternary phase-shift keying are also derived.**

***Index Terms*—Correlated fading, differential detection, phase-shift keying (PSK), pilot-aided coherent detection, postdetection diversity combining.**

I. Introduction

In MOBILE communications, there are several limiting factors for high data rate transmission, notably the availability of suitable radio-frequency (RF) spectrum and multipath propagation. Bandwidth-efficient modulation schemes such as M-ary phase-shift keying (M-PSK) can help to alleviate such problems, e.g., the global system for mobile communications (GSM) enhanced data rates for GSM evolution (EDGE) system is considering 8-PSK, whereas in wide-band code-division multiple-access (W-CDMA) system quaternary phase-shift keying (Q-PSK) has been selected for radio specifications [1]–[3]. However, it is known that the error performance of phase-shift keying (PSK) degrades with increased modulation levels, since high-level PSK is more sensitive to receiver noise. Furthermore, the hostile multipath-fading environment of the wireless communications further degrades receiver performance [4]–[7]. Therefore, the tradeoff between data rate and robustness of the transmission must always be examined carefully. In this respect, the choice of which demodulation techniques are employed must also be carefully chosen. It has been shown that the error performance for ideal coherent demodulation[1] of M-PSK (M-CPSK) is superior to that of differential coherent demodulation of differentially encoded M-PSK (M-DPSK) [8], [9]. In wireless communication applications, practical coherent demodulation can be achieved by using pilot-tone-aided (PTA) [10]–[18] and pilot-symbol-aided (PSA) [19]–[23] transmission techniques. In these techniques, a pilot (reference) signal is transmitted along with the data (information) signal. At the receiver, the received pilot is used as a phase and/or amplitude reference for coherent demodulation. However, extra bandwidth and transmit power are required to accommodate the pilot signal together with additional signal-processing algorithms and processing delay for channel estimation in the receiver. Due to these extra requirements, M-DPSK can be an attractive option for some low-cost architecture applications, despite the fact that the error performance of M-DPSK is inferior to that of coherent M-PSK.

It is well known that the performance of the receiver can be improved by using diversity reception techniques. However, diversity gain is reduced by increased correlation between the fading signals and/or unequal average signal power between diversity branches [4]–[7], [24], [25]. The diversity gain reduction may affect the overall performance of the system; hence, it is important for system engineers to predict the modem performance during the design and evaluation phases.

Error-probability expressions for diversity reception of M-PSK with unequal average power levels between diversity branches are given in [8], [9], [26], and [27]. Rayleigh-fading channel models are assumed in [26], whereas [8], [9], and [27] provide error expressions for a wider class of fading models, such as Rician and Nakagami models.

Performance analysis of diversity-combining reception for binary-level DPSK (B-DPSK) with correlated fading between diversity branches is given in [28]–[34]. References [28]–[31] assume a predetection diversity-combining technique, whereas [32]–[34] investigated the postdetection diversity-combining performance. Alouini and Simon [35] formulated the B- and Q-DPSK in Nakagami-fading channels with postdetection

Manuscript received May 15, 2002; revised May 13, 2003 and January 5, 2004.

The authors are with Telecommunication Research Laboratory, Toshiba Research Europe Ltd., Bristol, BS1 4ND, U.K. (e-mail: yuk.chow@toshiba-trel.com; joe.mcgeehan@toshiba-trel.com).

Digital Object Identifier 10.1109/TVT.2004.827160

[1]Ideal coherent demodulation is referred to the receiver that has perfect carrier phase and frequency references to perform demodulation.

diversity reception. Noneaker and Pursley [36] derived the upper and lower bounds for M-DPSK in Rician fading with postdetection diversity reception.

Performance of B-CPSK with correlated fading between diversity branches has been analyzed in [28]–[31], [37], and [38]. Error expressions for M-CPSK in Rayleigh- [39], [40] and Nakagami-fading [35] channels were also developed. However, all references were assumed to be ideal coherent demodulation only. In the case of pilot-aided M-CPSK systems, [36] discussed the extension of the analysis to PTA and PSA systems over Rician-fading channels. However, no analysis has been performed in this paper. Performance analysis of PSA B-CPSK over Rayleigh-fading channels with diversity reception has been studied in [41]. The effect of noisy channel estimation was included in the analysis, but only for the case of independent fading and equal average power between diversity branches.

By using the general error-probability formula for a quadratic receiver in a binary hypothesis test, between zero-mean complex Gaussian variables developed by Barrett [42] and the upper bound of symbol-error probability (SEP) derived in [43], upper-bounds SEP for multichannel reception with postdetection combining of M-DPSK, PTA, and PSA M-CPSK over frequency-flat Rayleigh-fading are formulated in this paper. The effect of correlated fading and unequal average power level between diversity branches are taken into account in the development. In addition, performance degradation due to imperfections in the demodulation process, such as the effects of Doppler spread on the M-DPSK scheme and noisy reference signal on PTA M-CPSK and PSA M-CPSK schemes are considered in the formulation.

II. System Modeling

The overall transmission system model with multichannel reception is shown in Fig. 1. The model assumes that there are D diversity channels, each carrying identical information. The fading in each branch is assumed to be frequency flat (or frequency nonselective) with envelope statistics that follow a Rayleigh distribution. Correlated fading between the D channels is assumed. The signal at the output of each channel is further corrupted by an additive white Gaussian noise (AWGN), which is assumed to be statistically independent on each channel. For mathematical convenience, an equivalent baseband (complex envelope) signal representation is used throughout the analysis.

A. Transmitted Signals

1) M-DPSK: In this system, the data (information) signals are differentially encoded before transmit. The equivalent baseband transmitted signal $u(t)$ of M-DPSK can be written as

$$u(t) = \sum_{n=-\infty}^{\infty} Ap(t - nT_s)e^{j\theta_n} \tag{1}$$

where θ_n is the transmitted phase at the nth time interval and A is the amplitude gain of $u(t)$. In M-DPSK, the information phase (phase angle of the data symbol i) at the nth time interval

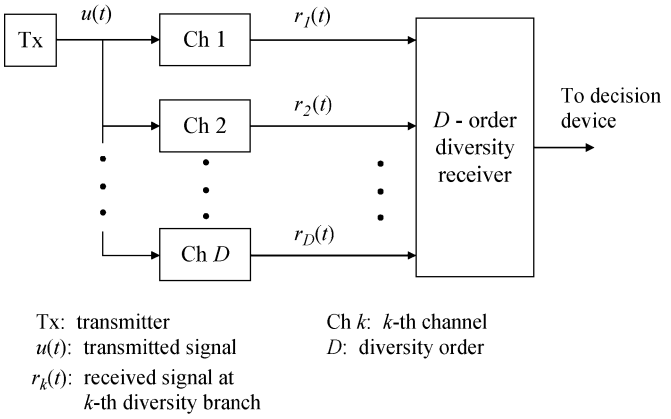

Fig. 1. Overall transmission model with multichannel reception.

$\Lambda_{i,n}$ is encoded in the phase difference between the two adjacent transmitted phases. Thus, the transmitted phase θ_n can be expressed as $\theta_n = \theta_{n-1} + \Lambda_{i,n}$, where

$$\Lambda_{i,n} = \frac{2\pi(i-1)}{M}, \qquad i = 1, 2, \ldots, M. \tag{2}$$

The index i denotes one of the M possible data symbols. The symbol duration is represented by T_s and $p(t)$ is the impulse response of a pulse-shaping filter with unity energy, i.e., $\int_{-\infty}^{\infty} |p(t)|^2 dt = 1$. Thus, the transmit energy per symbol $E_{s,\mathrm{Tx}} = (A^2/2)(\int_{-\infty}^{\infty} |p(t)|^2 dt) = A^2/2$ and the corresponding transmit power $P_{\mathrm{Tx}} = A^2/(2T_s)$.

2) PTA M-CPSK: In this system, a tone signal that is known to the receiver is transmitted along with the data signal. Based on pervious analysis given in [14]–[17], this paper assumes that Manchester encoding (also known as biphase line coding) is used to create a spectral null at the direct current (dc) level of data signal spectrum, so that the pilot tone can be inserted without interference to the data signal.[2] For PTA M-CPSK, the equivalent baseband transmitted signal $u(t)$ is the summation of the data signal $u_d(t) = \sum_{n=-\infty}^{\infty} A_d p(t - nT_s)e^{j\theta_n}$ and pilot signals $u_p(t) = A_p$, i.e.,

$$u(t) = u_d(t) + u_p(t). \tag{3}$$

In M-CPSK, the information phase ($\Lambda_{i,n}$) is encoded into the transmitted phase directly, i.e., $\theta_n = \Lambda_{i,n}$, [where $\Lambda_{i,n}$, is given in (2)]. The amplitudes of the data and pilot signals are denoted as A_d and A_p. Similar to the M-DPSK discussion, the total average transmit power is $P_{\mathrm{Tx}} = P_{\mathrm{Tx},d} + P_{\mathrm{Tx},p}$, where $P_{\mathrm{Tx},d} = A_d^2/(2T_s)$ and $P_{\mathrm{Tx},p} = A_p^2/2$ are the average transmit powers for the data and pilot signals. The ratio between the pilot and data signal powers is defined as η (i.e., $\eta = A_p^2 T_s/A_d^2$). Hence, for a given average transmit power P_{Tx}, the average transmit power for the data signal is $P_{\mathrm{Tx},d} = P_{\mathrm{Tx}}/(1+\eta)$. The corresponding transmit data-energy per symbol is $E_{s,d,\mathrm{Tx}} = E_{s,\mathrm{Tx}}/(1+\eta)$.

3) PSA M-CPSK: In this system, pilot symbols are transmitted along with the data symbols through the use of the

[2]Since the bandwidth of the Manchester encoded signal is double of the non-return-to-zero (NRZ) signal, a higher level modulation is required to compensate the effect of bandwidth expansion. Alternatively, a dual-tone calibration technique [12] or transparent tone-in-band technique [11], [13] can be applied.

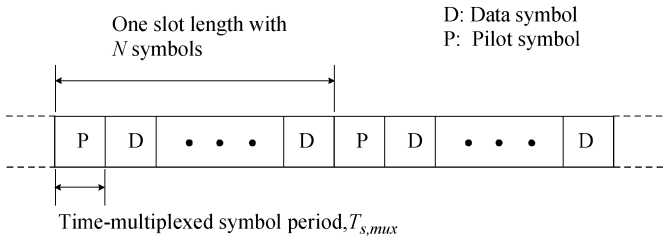

Fig. 2. Time-multiplexed sequence structure for PSA M-CPSK transmission.

time-multiplexing technique. Fig. 2 shows the structure of the time-multiplexed sequence in which one pilot symbol is periodically time multiplexed with $(N-1)$ data symbols, where N refers to a slot length. In order for pilot symbols to provide accurate channel estimation at the receiver, the pilot symbol insertion rate should be at least two times of the *Doppler spread* of the channel [20]–[23] and [41]. This implies that N is upper bounded by $N \leq (2 \times \text{Doppler spread} \times T_{s,\text{mux}})^{-1}$, where $T_{s,\text{mux}}$ represents the period of time-multiplexed symbol. The format of equivalent baseband transmitted signal $u(t)$ for PSA M-CPSK is same as the M-DPSK signal expressed in (1), with T_s replaced by $T_{s,\text{mux}}$ and θ_n equal to $\Lambda_{i,n}$ [where $\Lambda_{i,n}$ is defined in (2)]. The average transmit power for the data and pilot signals are $P_{\text{Tx},d} = A^2/(2T_{s,d})$ and $P_{\text{Tx},p} = A^2/(2T_{s,p})$, where $T_{s,d} = \kappa^{-1}T_{s,\text{mux}}$ and $T_{s,p} = NT_{s,\text{mux}}$ represent the effective data and pilot symbol periods. The parameter κ, which is the ratio between the number of data symbols and the time multiplexed symbols in one slot (i.e., $\kappa = (N-1)/N$), is called *slot efficiency*. The total average transmit power is $P_{\text{Tx}} = A^2/(2T_{s,\text{mux}})$ and the transmit energy per time-multiplexed symbol is $E_{s,\text{mux,Tx}} = A^2/2$. The corresponding transmit energy per data symbol can be expressed as $E_{\text{ds,Tx}} = \kappa^{-1}E_{s,\text{mux,Tx}}$.

B. Channel Model

For a frequency-flat Rayleigh-fading channel, the equivalent baseband received signal in the kth channel of a D-order diversity reception is given by

$$r_k(t) = g_k(t)u(t) + z_k(t), \qquad k = 1, 2, \ldots, D \tag{4}$$

where $g_k(t)$ represents the zero-mean complex Gaussian-fading process and $z_k(t)$ is the zero-mean complex AWGN with power spectral density of $2N_o$. The correlation function between $g_j(t)$ and $g_k(t)$ for $j, k = 1, \ldots, D$ is modeled as [36]

$$E\{g_j(t)g_k^*(t-\tau)\} = \begin{cases} \sigma_k^2\mu(\tau), & \text{for } k = j \\ \sigma_j\sigma_k\rho_{jk}\mu(\tau), & \text{for } k \neq j \end{cases} \tag{5}$$

where $E\{.\}$ denotes the ensemble average and the * indicates the complex conjugate. The parameter σ_k^2 is the average power gain of $g_k(t)$, $\mu(\tau)$ is the time-correlation function of the fading process that measures the similarities between $g_k(t)$ and $g_k(t-\tau)$, and ρ_{jk} is the complex cross-correlation coefficient between two fading processes $g_j(t)$ and $g_k(t)$. This model assumes that the time-correlation function is the same for each fading process and between two fading processes. The analysis also assumes that the fading variations are slow enough so that the Doppler spread is much smaller than the signaling rate and the fading process remains constant over one symbol interval, but varies to the next symbol. A parameter of interest is the *average power profile* for the D-order diversity channel defined by (in decibel scale)

$$H_p(D) = \left[\sigma_1^2, \quad \sigma_2^2, \quad \cdots, \quad \sigma_D^2\right] \tag{6}$$

which is useful to represent the unequal power gain between diversity channels.

C. Receiver Structure

Receiver structures for M-DPSK and pilot-aided M-PSK transmissions are outlined in this section and, more importantly, this section will show that the format of the decision variable for M-DPSK, PTA, and PSA M-CPSK detectors are equivalent. Ideal sample timing is assumed in the analysis.

1) M-DPSK: The M-DPSK receiver structure for the kth diversity branch is shown in Fig. 3(a). The received signal $r_k(t)$ is passed through a matched filter and the output of which is sampled at symbol rate R_s. The sampled outputs at nth and $(n-1)$th time intervals are U_k and K_k, which can be written in the form

$$\begin{aligned} U_k &= x_{U,k} + w_{U,k} \\ K_k &= x_{K,k} + w_{K,k} \end{aligned} \tag{7}$$

where $x_{U,k} = Ag_{k,n}\exp[j\theta_n]$, $w_{U,k} = z_{k,n}$, $x_{K,k} = Ag_{k,n-1}\exp[j\theta_{n-1}]$, and $w_{K,k} = z_{k,n-1}$. Variables $g_{k,n}$ and $z_{k,n}$ are the sampled outputs at nth time interval of $g(t)$ and $z(t)$ after the matched filtering. The *average received signal power-to-noise power ratio* (SNR) of U_k and K_k are

$$\gamma_{U,k} = \gamma_{K,k} = \frac{\sigma_k^2 A^2}{(2N_o).} \tag{8}$$

Since $(\sigma_k^2A^2)/2 = \sigma_k^2E_{s,\text{Tx}} = E_{s,\text{Rx},k}$ is the average received energy per symbol for the kth branch, the SNR of U_k and K_k are equivalent to the average received energy per symbol-to-noise power spectral density ratio for the kth branch, $\Gamma_{s,k}$, i.e.,

$$\gamma_{U,k} = \gamma_{K,k} = \frac{E_{s,\text{Rx},k}}{N_o} = \Gamma_{s,k}. \tag{9}$$

Therefore, the total average received energy per symbol-to-noise power spectral density ratio is $\Gamma_s = \sum_{k=1}^{D}\Gamma_{s,k}$.

2) PTA M-CPSK: The PTA M-CPSK receiver structure for the kth order diversity branch is shown in Fig. 3(b). The received signal $r_k(t)$ is passed into two paths, one for the data signal processing and the other for the pilot signal recovery. In the data-processing path, $r_k(t)$ is passed through a matched filter, the output of the which is sampled at symbol rate R_s. In the pilot signal recovery path, a pilot filter (PF) is used to extract the pilot signal from $r_k(t)$. In this analysis, the PF is assumed to be an ideal bandpass filter, i.e., the equivalent lowpass form of PF is an unity gain rectangular filter with bandwidth of $B_w/2$. To avoid distortion due to filtering, the value of B_w must be equal to or greater than the bandwidth of the power spectrum of the received pilot signal [14], [16], [17]. In the case of land mobile radio environments, the bandwidth of the received pilot-tone

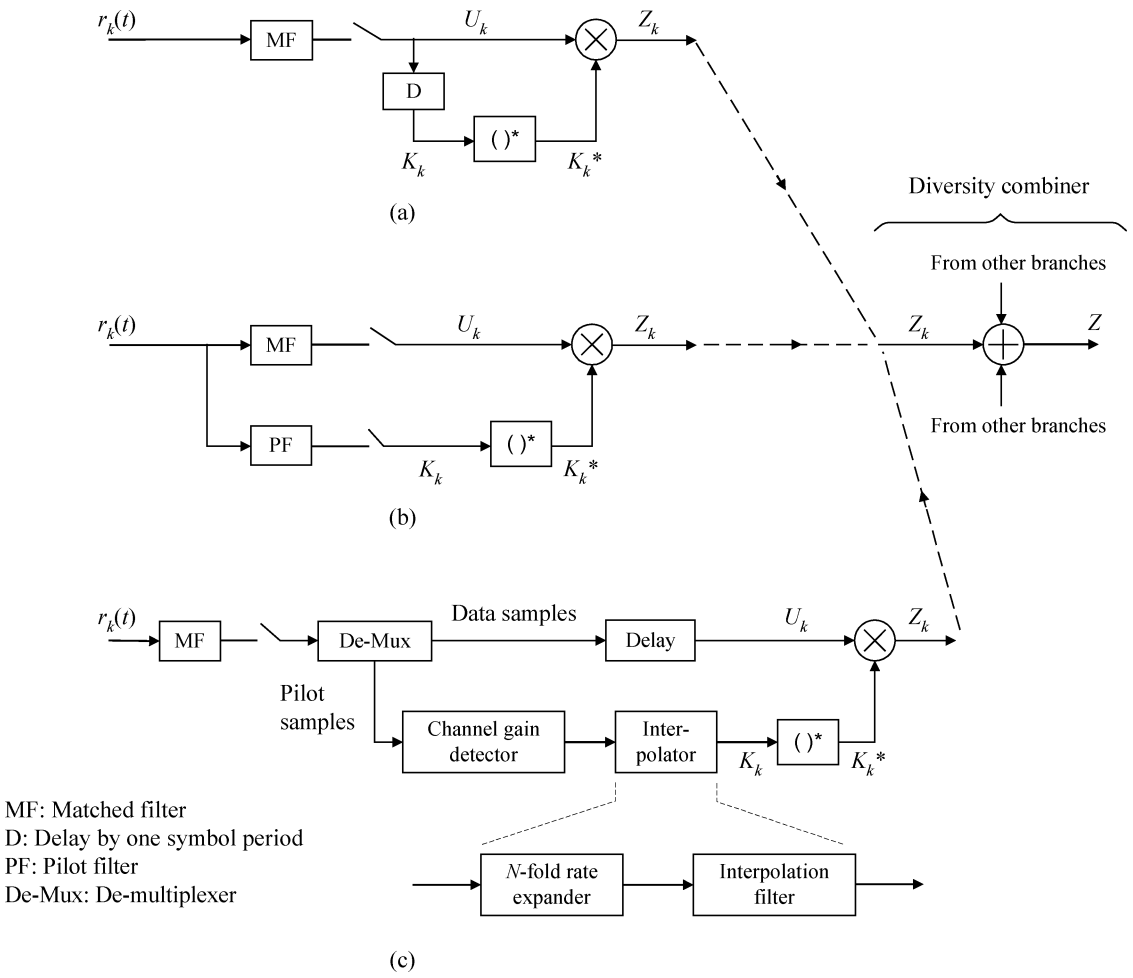

Fig. 3. Block diagrams for PSK receivers at the kth diversity branch. (a) M-DPSK, (b) PTA M-CPSK, and (c) PSA M-CPSK receivers.

signal-power spectrum can be spread up to twice of the maximum Doppler frequency f_D [5]. The sampled outputs at the nth time interval of data signal U_k and channel estimate K_k follow the form of (7) with $x_{U,k} = A_d g_{k,n} \exp[j\theta_n]$, $w_{U,k} = z_{d,k,n}$, $x_{K,k} = A_p g_{k,n}$, and $w_{K,k} = z_{p,k,n}$. Variables $g_{k,n}$ and $z_{d,k,n}$ are the sampled outputs at the nth time interval of $g(t)$ and $z(t)$ after the matched filtering. The noise sample at the output of the PF is represented as $z_{p,k,n}$, with power of $2N_oB_w$. The analysis assumes that the noise samples $z_{d,k,n}$ and $z_{p,k,n}$ are independent. The SNR of U_k and K_k are

$$\gamma_{U,k} = \frac{\sigma_k^2 A_d^2}{(2N_o)} \qquad \gamma_{K,k} = \frac{\sigma_k^2 A_p^2}{(2N_o B_w)}. \tag{10}$$

Since $(\sigma_k^2 A_d^2)/2 = \sigma_k^2\ E_{s,d,\mathrm{Tx}} = E_{s,d,\mathrm{Rx},k}$ is the average received data energy per symbol for the kth branch, the SNR of U_k is equivalent to the *average received data energy per symbol-to-noise power spectral density ratio for the kth branch* $\Gamma_{s,d,k}$, i.e.,

$$\gamma_{U,k} = \frac{E_{s,d,\mathrm{Rx},k}}{N_o} = \Gamma_{s,d,k}. \tag{11}$$

The SNR of U_k can also be expressed in terms of $\Gamma_{s,k}$ as

$$\gamma_{U,k} = \Gamma_{s,d,k} = \frac{\Gamma_{s,k}}{(1+\eta)}. \tag{12}$$

Therefore, the *total average received data energy per symbol-to-noise power spectral density ratio* is $\Gamma_{s,d} = \sum_{k=1}^{D} \Gamma_{s,d,k} = \Gamma_s/(1+\eta)$, where $\Gamma_s = \sum_{k=1}^{D} \Gamma_{s,k}$ is the *total average received energy per symbol-to-noise power spectral density ratio*.

3) PSA M-CPSK: The PSA M-CPSK receiver structure for the kth order diversity branch is shown in Fig. 3(c). The received signal $r_k(t)$ after the matched filtering and sampling is demultiplexed into two paths, one for data samples and the other for pilot samples. The received pilot samples are input to the channel gain detector in which the gain of the fading process is determined. A digital interpolator, which consists of an$N$-fold rate expander and a interpolation filter (INF), is used to estimate the gain of the fading process in the data position by interpolating the samples between the normalized pilot samples. Many types of INF have been considered in the past, such as simple Gaussian filters to more advanced Wiener filters [20], [22], [23]. In this analysis, an ideal INF is assumed, i.e., the INF is an ideal lowpass filter with frequency characteristic of

$$H(f) = \begin{cases} N, & \text{if } |f| \le \frac{B_w}{2} \\ 0, & \text{if } \frac{B_w}{2} < |f| \le \frac{R_{s,\mathrm{mux}}}{2} \end{cases} \tag{13}$$

where $B_w/2$ denotes the bandwidth of the INF and $R_{s,\mathrm{mux}} = 1/T_{s,\mathrm{mux}}$. To avoid distortion due to the filtering, the value of B_w must be equal to or greater than the Doppler spread (fading

bandwidth) of the channel. Sampled outputs at the nth time interval of data signal U_k and channel estimate K_k follow the form of (7) with $x_{U,k} = Ag_{k,n}\exp[j\theta_n]$, $w_{U,k} = z_{d,k,n}$, $x_{K,k} = Ag_{k,n}$, and $w_{K,k} = z_{i,k,n}$. Variables $g_{k,n}$ and $z_{d,k,n}$ are the sampled outputs at the nth time interval of $g(t)$ and $z(t)$ after the matched filtering. The noise sample at the output of the INF is represented as $z_{i,k,n}$ with the power of $2N_oNB_wT_{s,\mathrm{mux}}$. The analysis assumes that the noise samples $z_{d,k,n}$ and $z_{i,k,n}$ are independent. The corresponding SNR of U_k and K_k are

$$\gamma_{U,k} = \frac{\sigma_k^2 A^2}{(2N_o)} \qquad \gamma_{K,k} = \frac{\sigma_k^2 A^2}{(2N_oNB_wT_{s,\mathrm{mux}})}. \tag{14}$$

Since $(\sigma_k^2A^2)/2 = \sigma_k^2\ E_{s,\mathrm{mux,Tx}} = E_{s,\mathrm{mux,Rx},k}$ is the average received energy per time multiplexed symbol for the kth branch, the SNR of U_k is equivalent to the average received energy per time multiplexed symbol-to-noise power spectral density ratio for the k th branch, $\Gamma_{s,\mathrm{mux},k}$, i.e.,

$$\gamma_{U,k} = \frac{E_{s,\mathrm{mux,Rx},k}}{N_o} = \Gamma_{s,\mathrm{mux},k}. \tag{15}$$

The SNR of U_k can also be expressed in terms of average received energy per data symbol-to-noise power spectral density ratio for the kth branch $\Gamma_{\mathrm{ds},k}$

$$\gamma_{U,k} = \Gamma_{s,\mathrm{mux},k} = \frac{\kappa E_{\mathrm{ds,Rx},k}}{N_o} = \kappa\Gamma_{\mathrm{ds},k}. \tag{16}$$

Therefore, the total average received energy per time multiplexed symbol-to-noise power spectral density ratio is $\Gamma_{s,\mathrm{mux}} = \sum_{k=1}^{D}\Gamma_{s,\mathrm{mux},k} = \kappa\Gamma_{\mathrm{ds}}$, where $\Gamma_{\mathrm{ds}} = \sum_{k=1}^{D}\Gamma_{\mathrm{ds},k}$ is the total average received energy per data symbol-to-noise power spectral density ratio.

4) Diversity Combiner: Based on the analysis given above, it can be shown that if the transmission is ideal (i.e., no fading and AWGN), the phase of the demodulated signal $Z_k = U_kK_k^*$ is simply the phase of the actual transmitted symbol, where U_k and K_k are in the forms of (7) [where variables $x_{U,k}$, $w_{U,k}$, $x_{K,k}$, and $w_{K,k}$ used in (7) are given in Sections II-C-1, II-C-2, and II-C-3 for M-DPSK, PTA, and PSA M-CPSK). For D-order postdetection diversity, the combiner sums all the demodulator outputs and forms a combined vector Z, which can be expressed as

$$Z = \sum_{k=1}^{D} Z_k = \sum_{k=1}^{D} U_kK_k^*. \tag{17}$$

Therefore, Z can be used as a decision variable for M-DPSK, PTA, and PSA M-CPSK diversity receivers.

III. Error-Probability Analysis

Section II has shown that the format of the decision variables for M-DPSK, PTA, and PSA M-CPSK are equivalent [see (17)]. Therefore, a common analysis can be applied to formulate the SEP of the three modulation schemes. In the following analysis, intersymbol interference-free transmission and zero-frequency offset between transmitted carrier and receiver oscillator are assumed. Without a loss of generality, the information phase $\Lambda_{i,n} = 0$ can be assumed in the formulations.

A. Upper-Bound Formulation

1) Correlated Fading and Unequal Average Power Level Between Channels: Based on the analysis presented in [43], the upper bound of the SEP for M-DPSK, $P_s(M)$, can be expressed as

$$P_s(M) < 2\Pr\{V < 0\} \tag{18}$$

where

$$\Pr\{V<0\} = \Pr\left\{\sum_{k=1}^{D}(X_kY_k^* + X_k^*Y_k) < 0\right\} \tag{19}$$

represents the probability of random variable V is less than zero. The two random variables X_k and Y_k are defined as[3]

$$X_k = U_k \qquad Y_k = K_ke^{-j\Psi} \tag{20}$$

where $\Psi = \pi/2 - \pi/M$. Although the upper bound given in (18) is derived for M-DPSK, it is also suitable for the upper-bound development for PTA and PSA M-CPSK as well, since the format of decision variables are equivalent. The quadratic form $V = \sum_{k=1}^{D}(X_kY_k^* + X_k^*Y_k)$ in (19) can be expressed into a matrix form $V = \mathbf{w}^{\mathrm{H}}\mathbf{Q}\mathbf{w}$, where $\mathbf{w} = [X_1, Y_1, \ldots, X_D, Y_D]^{\mathrm{T}}$ is a complex vector with length of $2D$ and $\mathbf{Q} = \mathrm{diag}(\mathbf{J}_1, \mathbf{J}_2, \ldots, \mathbf{J}_D)$ is the $2D \times 2D$ block diagonal matrix,[4] with $\mathbf{J_k} = \begin{bmatrix} 0 & 1 \\ 1 & 0 \end{bmatrix}$ for $k = 1, 2, \ldots, D$. Hence, (19) can be written as

$$\Pr\{V<0\} = \Pr\{\mathbf{w}^{\mathrm{H}}\mathbf{Q}\mathbf{w} < 0\}. \tag{21}$$

The complex vector $\mathbf{w}$ has a zero-mean vector, i.e., $E\{\mathbf{w}\} = \mathbf{0}$, since both $g_{k,n}$ and $z_{k,n}$ are zero means (see Section II-B for definitions). Based on this particular setting, (21) can be solved by the technique proposed by Barrett [42]. The result is given as

$$\Pr\{V<0\} = \Pr\{\mathbf{w}^{\mathrm{H}}\mathbf{Q}\mathbf{w} < 0\} = \sum_{\substack{i \\ \lambda_i<0}}^{2\mathrm{D}} \prod_{\substack{j=1 \\ j\neq i}}^{2D} \frac{\lambda_i}{\lambda_i - \lambda_j} \tag{22}$$

where λ_i, for $i = 1, 2, \ldots, 2D$ are the eigenvalues of the matrix $\mathbf{CQ}$. The matrix $\mathbf{C}$ is the covariance matrix of $\mathbf{w}$.[5] Since $\mathbf{w}$ is a zero-mean complex vector, $\mathbf{C}$ is reduced to the correlation matrix, i.e., $E\{\mathbf{w}\mathbf{w}^{\mathrm{H}}\}$. Using (7) with $x_{U,k}$, $w_{U,k}$, $x_{K,k}$, and $w_{K,k}$ specified in Sections II-C-1, II-C-2, and II-C-3 for M-DPSK, PTA, and PSA M-CPSK covariance matrices for M-DPSK, PTA, and PSA M-CPSK schemes can be constructed as shown in Appendix I. The corresponding upper bound of SEP can be formulated by substituting (22) into (18).

[3]The rotation angle Ψ is used to rotate the decision variable Z [see (17)], so that decision error is equivalent to $V(= Ze^{j\Psi})$ is less than zero [43, Sec.3.2].

[4]Superscript H and T represent conjugate transpose and transpose of a matrix.

[5]A covariance matrix of a complex vector $\mathbf{x}$ is defined as $E\{(\mathbf{x} - \overline{\mathbf{x}})(\mathbf{x} - \overline{\mathbf{x}})^{\mathrm{H}}\}$, where $\overline{\mathbf{x}} = [E\{x_1\}, E\{x_2\}, \ldots, E\{x_N\}]^{\mathrm{T}}$ represents the mean vector of $\mathbf{x}$.

2) Independent Fading and Unequal Average Power Level Between Channels: In this particular case, the matrix $\mathbf{CQ}$ is reduced to a $2D \times 2D$ block diagonal matrix, which can be represented as $\mathrm{diag}(\mathbf{A}_1, \mathbf{A}_2, \ldots, \mathbf{A}_D)$, where

$$\mathbf{A}_k = \begin{bmatrix} E\{X_k Y_k^*\} & E\{|X_k^2|\} \\ E\{|Y_k^2|\} & E\{X_k^* Y_k\} \end{bmatrix}, \qquad k = 1, 2, \ldots, D. \tag{23}$$

Based on the covariance function between X_k and Y_k, which is given in Appendix I, the corresponding eigenvalues of $\mathbf{CQ}$ are $\lambda^{(\mathbf{A})} = \{\lambda_1^{(\mathbf{A}_1)}, \lambda_2^{(\mathbf{A}_1)}, \ldots, \lambda_1^{(\mathbf{A}_D)}, \lambda_2^{(\mathbf{A}_D)}\}$, where $\{\lambda_1^{(\mathbf{A}_k)}, \lambda_2^{(\mathbf{A}_k)}\}$ for $k = 1 \ldots D$, (see Appendix II for the derivation)

$$\begin{Bmatrix} \lambda_1^{(\mathbf{A}_k)} \\ \lambda_2^{(\mathbf{A}_k)} \end{Bmatrix} = \begin{cases} \mu_s \Gamma_{s,k} \sin\left(\frac{\pi}{M}\right) \\ \pm\sqrt{(\Gamma_{s,k}+1)^2 - \left(\mu_s \Gamma_{s,k} \cos\left(\frac{\pi}{M}\right)\right)^2}, & \text{DPSK} \\ \sqrt{R_s}\left[\Gamma_{s,d,k}\sqrt{\eta}\sin\left(\frac{\pi}{M}\right) \pm\sqrt{\Xi_{\mathrm{PTA}} - \eta\Gamma_{s,d,k}^2 \cos^2\left(\frac{\pi}{M}\right)}\right], & \text{PTA CPSK} \\ \Gamma_{s,\mathrm{mux},k}\sin\left(\frac{\pi}{M}\right) \\ \pm\sqrt{\Xi_{PSA} - \Gamma_{s,\mathrm{mux},k}^2 \cos^2\left(\frac{\pi}{M}\right)}, & \text{PSA CPSK} \end{cases} \tag{24}$$

with $\Xi_{\mathrm{PTA}} = (\Gamma_{s,d,k} + 1)(\eta\Gamma_{s,d,k} + \beta_p)$ and $\Xi_{\mathrm{PSA}} = (\Gamma_{s,\mathrm{mux},k} + 1)(\Gamma_{s,\mathrm{mux},k} + N\beta_i)$. The parameter $\mu_s = \mu(T_s)$ represents the time-correlation coefficient of the fading process between two successive symbols, $\Gamma_{s,d,k} = \Gamma_{s,k}/(1+\eta)$, $\beta_p = B_w/R_s$ is the normalized PF bandwidth, $\Gamma_{s,\mathrm{mux},k} = \kappa\Gamma_{\mathrm{ds},k}$, N is the number of time multiplexed symbols per slot, and $\beta_i = B_w/R_{s,\mathrm{mux}}$ is the normalized INF bandwidth. The upper-bound SEP of the three modulation schemes can be calculated by using (18) together with (22) and (24). It should be noted that in order to obtain meaningful results, all eigenvalues of $\mathbf{CQ}$ must be distinct; otherwise, (22) will fail. This implies that the above result is only applicable to unequal average power between diversity branches.

3) Single-Channel Reception ($D = 1$): In this case, (22) is simplified to $\Pr\{V < 0\} = \lambda_2/(\lambda_2 - \lambda_1)$, assuming that $\lambda_2 < 0$. The matrix $\mathbf{CQ}$ is reduced to a 2×2 matrix as in the form of (23) (i.e., $k = 1$). By using λ_1 and λ_2 from (37) (see Appendix II), $\Pr\{V < 0\}$ can now be expressed as

$$\begin{aligned} &\Pr\{V < 0\} \\ &= \frac{1}{2}\left(1 - \frac{\mathrm{Re}\{\mathrm{E}\{\mathrm{X}_1\mathrm{Y}_1^*\}\}}{\sqrt{E\{|X_1^2|\}\,E\{|Y_1^2|\} - (\mathrm{Im}\{E\{X_1 Y_1^*\}\})^2}}\right) \\ &= \frac{(1-F)}{2}. \end{aligned} \tag{25}$$

Hence, the upper-bound SEP given in (18) is simplified to

$$P_s(M) < 1 - F. \tag{26}$$

Based on the covariance function given in (33)–(35) (see Appendix I), for M-DPSK, PTA M-CPSK, and PSA M-CPSK, the parameter F in (25) and (26) can be written as

$$F = \begin{cases} \frac{\mu_s \Gamma_s \sin\left(\frac{\pi}{M}\right)}{\sqrt{(\Gamma_s+1)^2 - \mu_s^2\Gamma_s^2\cos^2\left(\frac{\pi}{M}\right)}}, & \text{DPSK} \\ \frac{\sqrt{\Gamma_{s,d}}\sqrt{\eta\Gamma_{s,d}}\sin\left(\frac{\pi}{M}\right)}{\sqrt{\Xi_{PTA} - \eta\Gamma_{s,d}^2\cos^2\left(\frac{\pi}{M}\right)}}, & \text{PTA CPSK} \\ \frac{\Gamma_{s,\mathrm{mux}}\sin\left(\frac{\pi}{M}\right)}{\sqrt{\Xi_{PSA} - \Gamma_{s,\mathrm{mux}}^2\cos^2\left(\frac{\pi}{M}\right)}}, & \text{PSA CPSK} \end{cases} \tag{27}$$

with $\Xi_{\mathrm{PTA}} = (\Gamma_{s,d}+1)(\eta\Gamma_{s,d} + \beta_p)$ and $\Xi_{\mathrm{PSA}} = (\Gamma_{s,\mathrm{mux}} + 1)(\Gamma_{s,\mathrm{mux}} + N\beta_i)$.

B. Exact Bit-Error Probability (BEP) for Binary and Quaternary Level PSK

Reference [43] has shown that the exact BEP of binary- and quaternary-level PSK with Gray coding can be formulated as[6]

$$\begin{aligned} P_b(2) &= \Pr\{V < 0\}, \qquad \text{with } \Psi = 0 \\ P_b(4) &= \Pr\{V < 0\}, \qquad \text{with } \Psi = \frac{\pi}{4}. \end{aligned} \tag{28}$$

Exact BEP expressions for B-, Q-DPSK, PTA, and PSA B-, Q-CPSK can be evaluated by substituting (22) into (28).

1) BEP of DPSK With $D = 1$: Based on (25) and (28), the BEP for B- and Q-DPSK can be derived as

$$\begin{aligned} P_b(2) &= \frac{\left\{1 - \mu_s\Gamma_s(\Gamma_s+1)^{-1}\right\}}{2} \\ P_b(4) &= \frac{\left\{1 - \mu_s\Gamma_s\left[2(\Gamma_s+1)^2 - (\mu_s\Gamma_s)^2\right]^{-\frac{1}{2}}\right\}}{2}. \end{aligned} \tag{29}$$

The above BEP expressions for B- and Q-DPSK are equivalent to (79) and (87) of [43], although written in a different form. Both expressions reduce to the results given in (8.173) and (8.174) of [9] if zero Doppler spread is assumed (i.e., $\mu_s = 1$).

2) BEP of PTA CPSK With $D = 1$: The BEP for PTA B and Q-CPSK can be expressed as

$$\begin{aligned} P_b(2) &= \frac{\left\{1 - \Gamma_{s,d}\left[(\Gamma_{s,d}+1)(\Gamma_{s,d} + \beta_p\eta^{-1})\right]^{-\frac{1}{2}}\right\}}{2} \\ P_b(4) &= \frac{\left\{1 - \Gamma_{s,d}\left[2(\Gamma_{s,d}+1)(\Gamma_{s,d} + \beta_p\eta^{-1}) - \Gamma_{s,d}^2\right]^{-\frac{1}{2}}\right\}}{2} \end{aligned} \tag{30}$$

where $\Gamma_{s,d} = \Gamma_s/(1+\eta)$. Although written in a different form, the BEP expression for PTA B-CPSK given above is equivalent to (71) of [15] and (43) of [16]. If the PF output is noise free and all available power is allocated to the data signal (i.e., $\beta_p = 0$ and $\eta \to 0$), (30) approaches the expression for ideal coherent detection [8].

[6]The equations assume that the information phase $\Lambda_{i,n} = 0$ for both binary- and quaternary-level PSK and zero frequency offset between the transmitter and receiver oscillator.

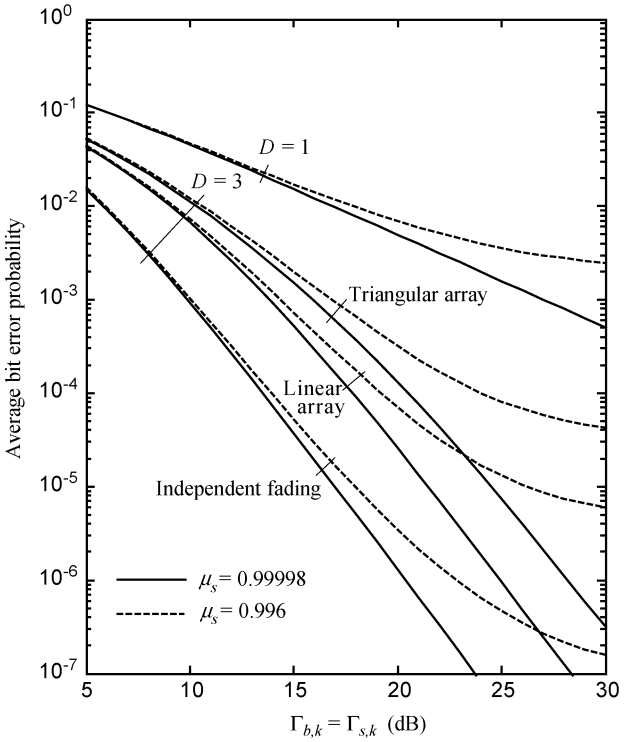

Fig. 4. Error performance of B-DPSK in frequency-flat Rayleigh-fading channels with D-order diversity receptions. Correlated fading is assumed in both the triangular and uniform linear-array formations. μ_s is the time-correlation of the fading process between two successive symbols.

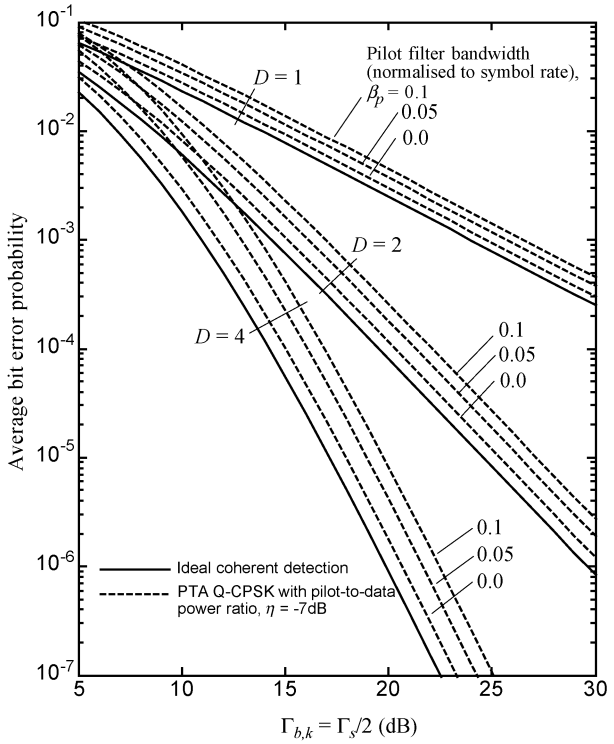

Fig. 5. Error performance of PTA Q-CPSK in frequency-flat Rayleigh-fading channels with multichannel receptions. The relative average power profile (in decibels) for second- and fourth-order diversity reception are $H_p(2) = [0, -3]$ and $H_p(4) = [0, -3, -5, -10]$. Independent fading between diversity branches is assumed.

3) BEP of PSA CPSK With $D = 1$: BEP for PSA B and Q-CPSK can be expressed in terms of $\Gamma_{\rm ds}$ as

$$P_b(2) = \frac{\left\{1 - \Gamma_{\rm ds}\left[(\Gamma_{\rm ds} + \kappa^{-1})(\Gamma_{\rm ds} + N\beta_i\kappa^{-1})\right]^{-\frac{1}{2}}\right\}}{2}$$
$$P_b(4) = \frac{\left\{1 - \Gamma_{\rm ds}\left[2(\Gamma_{\rm ds} + \kappa^{-1})(\Gamma_{\rm ds} + N\beta_i\kappa^{-1}) - \Gamma_{\rm ds}^2\right]^{-\frac{1}{2}}\right\}}{2} \quad (31)$$

where κ is the slot efficiency that is defined in Section II-A-3. The BEP expression for B-PSK is equivalent to the one given in [21] and [41]. In the case of the Q-PSK expression, an equivalent expression has been derived by [21]. If the INF output is noise free and the slot length $N \gg 1$, i.e., $\beta_i = 0$ and $\kappa \to 1$, (31) approaches the expression for ideal coherent detection [8].

IV. Numerical Results and Discussion

A. Exact BEP for B- and Q-Level PSK

Numerical results for the average BEP of B-DPSK in correlated Rayleigh-fading channels with third-order diversity reception were evaluated in [32]. Both triangular and uniform linear antenna array configurations with specified power cross-correlation values between antenna branches were considered [see (52) and (53) of [32])]. The analysis assumed that the equal power level between all diversity channels and the fading is slow enough so that the channel gain remains constant for two successive symbol periods (i.e., $\mu_s = 1.0$). Using the B-DPSK expression [see (28)], derived in the last section [with ρ_{jk} equals to the square root of the power correlation coefficient given in (52) and (53) of [32], Fig. 4 reproduces the average BEP of B-DPSK for both triangular and linear antenna array configurations. To approximate the equal diversity channel power and slow-fading conditions, the average power profile for the three diversity channels and the time-correlation of the fading process between two successive symbols are set to $H_p(3) = [0, -0.1, -0.2]$ and $\mu_s = 0.99998$ in the calculation. Results given in Fig. 4 are in good agreement with the numerical results presented in [32, Fig. 4]. When compared to the independent fading, the error performance degradation due to the correlated fading between diversity branches is evident. The graph also shows that the BEP of DPSK degrades further when the time-correlation value between the two symbols decreases.

Fig. 5 shows the average BEP of PTA Q-CPSK for various diversity order and normalized PF bandwidth β_p. Independent fading and unequal average power level between diversity channels with $H_p(2) = [0, -3]$ and $H_p(4) = [0, -3, -5, -10]$ are considered. The pilot-to-data power ratio η is fixed to -7 dB for all cases. The BEP curves for ideal coherent demodulated Q-PSK, derived in [8], are also given in Fig. 5. Results show the performance loss of using pilot-aided technique and the effects of noisy reference signal for channel estimation. Although not shown in the graph, the BEP of PTA Q-CPSK approaches to ideal coherent demodulation of Q-PSK when $\beta_p = 0$ and $\eta \to -\infty$ dB.

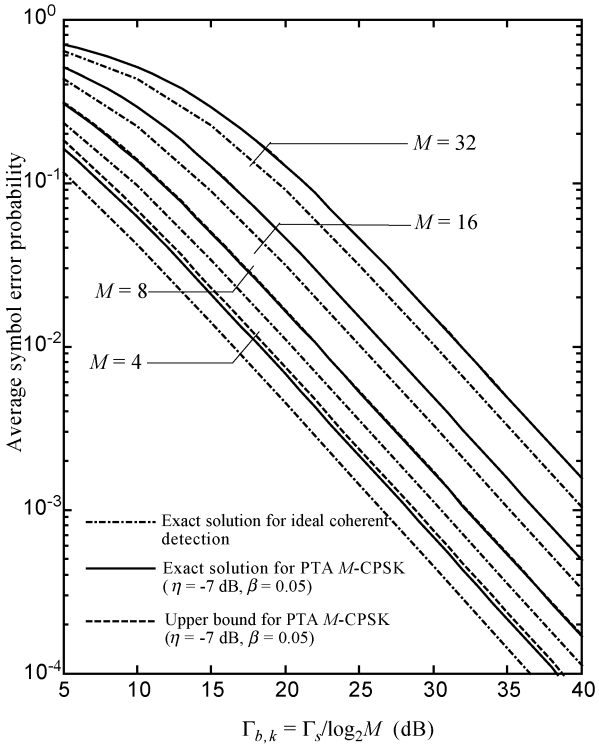

Fig. 6. Comparison of average SEP of PTA M-CPSK with exact and upper-bound solutions in frequency-flat Rayleigh-fading channels (without diversity receptions, i.e., $D = 1$). The time correlation of the fading process between two successive symbols μ_s is set to 1.0 (i.e., zero Doppler spread).

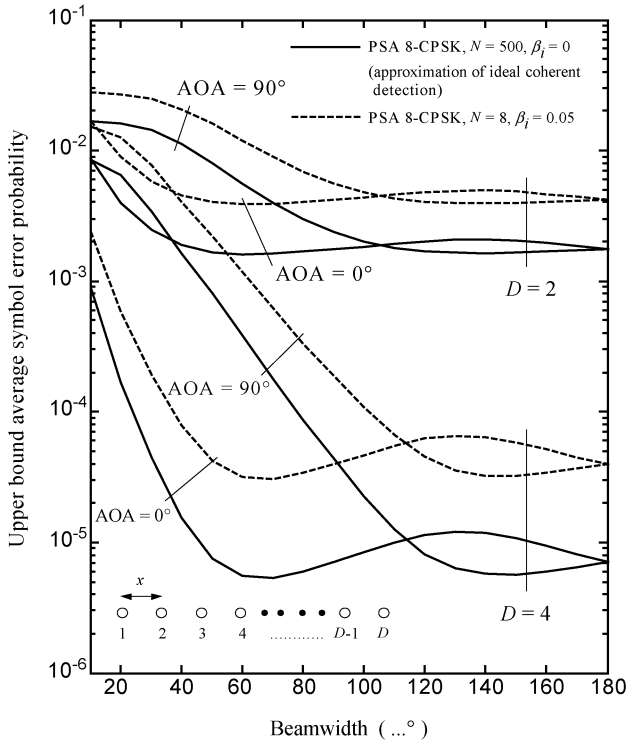

Fig. 7. Error performance of PSA 8-CPSK in frequency-flat Rayleigh-fading channels with two- and four-branch uniform linear antenna-array receptions. The average SEP is a function of beamwidth and AOA. The antenna spacing x is set to half of carrier wavelength and $\Gamma_{\mathrm{ds},k} = 20$ dB. The relative average power profile (in decibels) is $H_p(2) = [0, -0.1]$ and $H_p(4) = [0, -0.1, -0.15, -0.2]$.

B. Upper-Bound SEP for M-ary Level PSK

Exact and upper-bound SEP of PTA 4, 8, 16, and 32 CPSK with single-channel reception are illustrated in Fig. 6. The parameters η and β_p are fixed to -7 dB and 0.05 for all cases. The exact SEP are calculated by using (70) in [15] where single integration is required. The upper bounds are calculated by using (26). Results show the improvement of the bound when the modulation level increases. For $M > 8$, the difference between the exact and upper-bound curves is unnoticeable. The average SEP for the ideal coherent demodulations are also presented as references. The result illustrates the performance degradation due to pilot-aided transmission.

Recently, the error performance of ideal coherent demodulated M-PSK with uniform linear antenna array reception has been analyzed in [40]. The effects of correlated fading due to antenna spacing and operating environments, such as angle of- arrival (AOA) and beamwidth of incoming signals, were considered. The antenna array's cross-correlation model used in [40] has a property of $\rho_{kj} = \rho_{jk}{}^*$, for $j, k = 1, \ldots, D$. By using the same cross-correlation model, Fig. 7 shows the upper-bound SEP of PSA 8-CPSK as a function of beamwidth for two- and four-branch linear antenna array reception. The antenna spacing of one-half of carrier wavelength, AOA of 0° (broadside) and 90° (end fire), and $\Gamma_{\mathrm{ds},k} = 20\,\mathrm{dB}$ are considered. Numerical results for the upper-bound SEP of PSA 8-CPSK with $N = 500$ and $\beta_i = 0$ (approximation of ideal coherent demodulation) are in good agreement with the exact solutions obtained in [40, Fig. 3]. The results also show the performance degradation due to the redundancy of pilot symbols and noise channel estimation.

C. Imperfect Correlation Between Channel Estimate and Data Signal

This effect is already addressed in the M-DPSK analysis, where imperfect correlation between the previous signal (channel estimate) K_k and current signal (data signal) U_k is due to the imperfect time correlation of the fading process μ_s. In the case of pilot-aided M-CPSK analysis, perfect correlation between channel estimate and data signal is assumed in Section II-C. However, this assumption is not valid when the bandwidth of PF and INF is narrower than the bandwidth of the fading spectrum [16], [17], [20]–[22]. By following the analysis given in [16], the effect of decorrelation between the channel estimate and data signal on PTA system can be incorporated by modifying the covariance matrix $\mathbf{C}$. As in Section II-C.2, assuming that the equivalent lowpass PF is an unity gain rectangular filter with bandwidth of $B_w/2$, the elements $E\{|Y_k^2|\}$ are modified to $\varepsilon\eta\Gamma_{s,d,k}R_s + B_w$, where $\varepsilon = \int_{-B_w/2}^{B_w/2} S_g(f)\mathrm{df}$ and has a range of $0 \le \varepsilon \le 1$. $S_g(f)$ is the normalized power spectral density of the fading process $g_k(t)$ with fading bandwidth of $B_g/2$. The parameter ε is also required in $E\{X_k\ Y_k{}^*\}$, $E\{Y_j\ Y_k{}^*\}$, and $E\{X_j\ Y_k{}^*\}$, as well as in their complex conjugate pairs. Fig. 8 shows the BEP of PTA Q-CPSK with different values of ν (the ratio of B_w to B_g). In the calculation, land mobile radio channel model with the "U"-shape power spectral density (i.e., $S_g(f) = [\pi(f_D^2 - f^2)^{1/2}]^{-1}$) [7] and normalized maximum Doppler frequency $(f_D T_s)$ of 0.04 were assumed. For this model, $\nu = B_w/(2f_D)$, $\beta_p = 2\nu f_D T_s$,

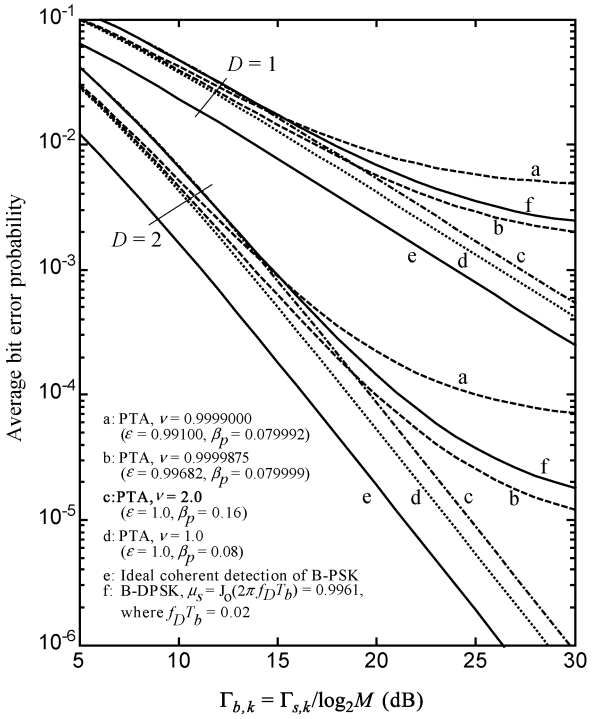

Fig. 8. Error performance of PTA Q-CPSK as a function of ν (PF bandwidth to fading bandwidth ratio B_w/B_g). Rectangular PF $\eta = -7$ dB, land mobile radio channel model with $f_D T_s$ of 0.04, and independent fading between diversity branches is assumed.

and $\varepsilon = (2/\pi)\arcsin(\min(1,\nu))$. Performance degradation due to decorrelation between the channel estimate and data signal on PTA Q-CPSK is illustrated in Fig. 8. Results show that the error performance is very sensitive to the band edge distortion (i.e., for $\nu < 1$). This is due to the fact that the "U"-shape spectrum has high proportion of power near $\pm f_D$ [16]. This figure also shows the BEP curves for ideal coherent demodulation B-PSK and B-DPSK with $\mu_s = J_0(2\pi f_D T_b)$, where $J_0(.)$ is the zero-order Bessel function of the first kind and T_b represents the bit period. Results given in Fig. 8 provide BEP comparison between the three transmission techniques under common transmit information bit rate and occupied bandwidth conditions.

V. Conclusion

In this paper, upper-bound expressions for SEPs of M-DPSK, PTA, and PSA M-CPSK over frequency-flat Rayleigh-fading channels have been formulated. Postdetection maximal-ratio combining technique is assumed at the receiver. The derived upper bounds are able to investigate the effect of AWGN, correlated fading, and unbalanced power level between diversity branches. The effect of Doppler spread on M-DPSK detection, noisy-channel estimation on PTA, and PSA M-CPSK detections are also taken into account in the formulations. Expressions to calculate the exact bit-error probability of binary and quaternary DPSK, PTA, and PSA CPSK are also evaluated. To validate the accuracy of the upper bound, comprehensive sets of numerical results produced by the upper bound have been compared with the previous published results.

Appendix I
Covariance Functions

The $2D \times 2D$ covariance matrix $\mathbf{C}$ described in Section III is defined by

$$\mathbf{C} = E\left\{\begin{bmatrix} |X_1^2| & X_1Y_1^* & \cdots & X_1X_D^* & X_1Y_D^* \\ X_1^*Y_1 & |Y_1^2| & & Y_1X_D^* & Y_1Y_D^* \\ \vdots & & \ddots & & \vdots \\ X_1^*X_D & Y_1^*X_D & & |X_D^2| & X_DY_D^* \\ X_1^*Y_D & Y_1^*Y_D & \cdots & X_D^*Y_D & |Y_D^2| \end{bmatrix}\right\}. \tag{32}$$

All matrix elements in $\mathbf{C}$ can be derived by using (7) [where variables $x_{U,k}$, $w_{U,k}$, $x_{K,k}$, and $w_{K,k}$ used in (7) are given in Sections II-C-1, II-C-2, and II-C-3 for M-DPSK, PTA, and PSA M-CPSK] and along with the channel covariance function specified in (5). The corresponding covariance elements for M-DPSK, PTA, and PSA M-CPSK schemes are derived below. All expressions below are normalized to $2N_o$ so that results can be expressed in terms of SNR at the kth diversity branch. In the following, zero frequency offset between transmitter and receiver oscillators is assumed.

M-DPSK: Covariance between X_j, Y_j, X_k, and Y_k for diversity branch j and k is

$$\begin{aligned} E\{|X_k^2|\} &= E\{|U_k^2|\} = \Gamma_{s,k} + 1 \\ E\{|Y_k^2|\} &= E\{|K_k^2|\} = \Gamma_{s,k} + 1 \\ E\{X_kY_k^*\} &= E\{U_kK_k^*\}e^{j\Psi} = \Gamma_{s,k}\mu_s e^{j\Psi} \\ E\{X_k^*Y_k\} &= (E\{X_kY_k^*\})^* \\ E\{X_jX_k^*\} &= E\{U_jU_k^*\} = \rho_{jk}(\Gamma_{s,j})^{\frac{1}{2}}(\Gamma_{s,k})^{\frac{1}{2}} \\ E\{X_j^*X_k\} &= (E\{X_jX_k^*\})^* \\ E\{Y_jY_k^*\} &= E\{K_jK_k^*\} = \rho_{jk}(\Gamma_{s,j})^{\frac{1}{2}}(\Gamma_{s,k})^{\frac{1}{2}} \\ E\{Y_j^*Y_k\} &= (E\{K_jK_k^*\})^* \\ E\{X_jY_k^*\} &= E\{U_jK_k^*\}e^{j\Psi} = \rho_{jk}\mu_s(\Gamma_{s,j})^{\frac{1}{2}}(\Gamma_{s,k})^{\frac{1}{2}}e^{j\Psi} \\ E\{X_j^*Y_k\} &= (E\{X_jY_k^*\})^* \end{aligned} \tag{33}$$

where $\Gamma_{s,k}$ is given in (9).

PTA M-CPSK: Covariance between X_j, Y_j, X_k, and Y_k for diversity branch j and k is

$$\begin{aligned} E\{|X_k^2|\} &= E\{|U_k^2|\} = \Gamma_{s,d,k} + 1 \\ E\{|Y_k^2|\} &= E\{|K_k^2|\} = \eta\Gamma_{s,d,k}R_s + B_w \\ E\{X_kY_k^*\} &= E\{U_kK_k^*\}e^{j\Psi} = \Gamma_{s,d,k}\sqrt{\eta R_s}e^{j\Psi} \\ E\{X_k^*Y_k\} &= (E\{X_kY_k^*\})^* \\ E\{X_jX_k^*\} &= E\{U_jU_k^*\} = \rho_{jk}\sqrt{\Gamma_{s,d,j}}\sqrt{\Gamma_{s,d,k}} \\ E\{X_j^*X_k\} &= (E\{X_jX_k^*\})^* \\ E\{Y_jY_k^*\} &= E\{K_jK_k^*\} = \rho_{jk}\eta R_s\sqrt{\Gamma_{s,d,j}}\sqrt{\Gamma_{s,d,k}} \\ E\{Y_j^*Y_k\} &= (E\{K_jK_k^*\})^* \\ E\{X_jY_k^*\} &= E\{U_jK_k^*\}e^{j\Psi} = \rho_{jk}\sqrt{\Gamma_{s,d,j}}\sqrt{\eta\Gamma_{s,d,k}R_s}e^{j\Psi} \\ E\{X_j^*Y_k\} &= (E\{X_jY_k^*\})^* \end{aligned} \tag{34}$$

where $\Gamma_{s,d,k}$ is given in (11).

PSA M-CPSK: Covariance between X_j, Y_j, X_k, and Y_k for diversity branch j and k is

$$\begin{aligned}
E\left\{\left|X_k^2\right|\right\} &= E\left\{\left|U_k^2\right|\right\} \\
&= \Gamma_{s,\mathrm{mux},k} + 1 \\
E\left\{\left|Y_k^2\right|\right\} &= E\left\{\left|K_k^2\right|\right\} \\
&= \Gamma_{s,\mathrm{mux},k} + \frac{(NB_w)}{R_{s,\mathrm{mux}}} \\
E\left\{X_k Y_k^*\right\} &= E\left\{U_k K_k^*\right\} e^{j\Psi} \\
&= \Gamma_{s,\mathrm{mux},k} e^{j\Psi} \\
E\left\{X_k^* Y_k\right\} &= \left(E\left\{X_k Y_k^*\right\}\right)^* \\
E\left\{X_j X_k^*\right\} &= E\left\{U_j U_k^*\right\} \\
&= \rho_{jk}(\Gamma_{s,\mathrm{mux},j})^{\frac{1}{2}}(\Gamma_{s,\mathrm{mux},k})^{\frac{1}{2}} \\
E\left\{X_j^* X_k\right\} &= \left(E\left\{X_j X_k^*\right\}\right)^* \\
E\left\{Y_j Y_k^*\right\} &= E\left\{K_j K_k^*\right\} \\
&= \rho_{jk}(\Gamma_{s,\mathrm{mux},j})^{\frac{1}{2}}(\Gamma_{s,\mathrm{mux},k})^{\frac{1}{2}} \\
E\left\{Y_j^* Y_k\right\} &= \left(E\left\{K_j K_k^*\right\}\right)^* \\
E\left\{X_j Y_k^*\right\} &= E\left\{U_j K_k^*\right\} e^{j\Psi} \\
&= \rho_{jk}(\Gamma_{s,\mathrm{mux},j})^{\frac{1}{2}}(\Gamma_{s,\mathrm{mux},k})^{\frac{1}{2}} e^{j\Psi} \\
E\left\{X_j^* Y_k\right\} &= \left(E\left\{X_j Y_k^*\right\}\right)^*
\end{aligned} \tag{35}$$

where $\Gamma_{s,\mathrm{mux},k}$ is given in (15).

Appendix II
Eigenvalues of Block Diagonal Matrices

A $2D \times 2D$ block diagonal matrix $\mathbf{C} = \mathrm{diag}(\mathbf{A}_1, \mathbf{A}_2, \ldots, \mathbf{A}_D)$ with $\mathbf{A_k} = \begin{bmatrix} a_k & x_k \\ y_k & a_k^* \end{bmatrix}$ for $k = 1, 2, \ldots, D$, where a_k is a complex variable and x_k and y_k are real variables. The corresponding eigenvalues of $\mathbf{C}$ are

$$\lambda^{(\mathbf{A})} = \left\{\lambda_1^{(\mathbf{A}_1)}, \lambda_2^{(\mathbf{A}_1)}, \ldots, \lambda_1^{(\mathbf{A}_D)}, \lambda_2^{(\mathbf{A}_D)}\right\} \tag{36}$$

where

$$\begin{Bmatrix} \lambda_1^{(\mathbf{A}_k)} \\ \lambda_2^{(\mathbf{A}_k)} \end{Bmatrix} = \mathrm{Re}\{a_k\} \pm \sqrt{x_k y_k - (\mathrm{Im}\{a_k\})^2}. \tag{37}$$

Acknowledgment

The authors are grateful to M. Fitton, M. Ismail, and K. Rizvi, Toshiba Research Europe Limited, Bristol, U.K., for their valuable comments and suggestions in relation to the preparation of this paper. The authors would also like to thank the reviewers for their valuable and constructive comments, which improved the accuracy and presentation of this paper.

References

[1] A. Furuskar, S. Mazur, F. Muller, and H. Olofsson, "EDGE: Enhanced data rakes for GSM and TDMA/136 evolution," *IEEE Pers. Commun.*, vol. 6, pp. 56–66, June 1999.

[2] M. Zeng, A. Annamalai, and V. K. Bhargava, "Recent advances in cellular wireless communications," *IEEE Commun. Mag.*, vol. 37, pp. 128–138, Sept. 1999.

[3] H. Holma and A. Toskala, Eds., *WCDMA for UMTS: Radio Access for Third Generation Mobile Communications*. West Sussex, U.K.: Wiley, 2000.

[4] M. Schwartz, W. R. Bennett, and S. Stein, *Communication Systems and Techniques*. New York: McGraw-Hill, 1966.

[5] W. C. Jakes, Jr., Ed., *Microwave Mobile Communications*. New York: Wiley, 1974.

[6] W. C. Y. Lee, *Mobile Communications Engineering*. New York: McGraw-Hill, 1982.

[7] J. D. Parsons and J. G. Gardiner, *Mobile Communications Systems*. Glasgow, U.K.: Blackie and Son, 1989.

[8] J. P. Proakis, *Digital Communications*, 3rd ed. New York: McGraw-Hill, 1995.

[9] M. K. Simon and M.-S. Alouini, *Digital Communication Over Fading Channels: A Unified Approach to Performance Analysis*. New York: Wiley, 2000.

[10] A. Bateman and J. McGeehan, "Data transmission over UHF fading mobile radio channels," *Proc. Inst. Elect. Eng.*, pt. F, pp. 364–374, July 1984.

[11] J. P. McGeehan and A. Bateman, "Phase locked transparent tone-in-band (TTIB): A new spectrum configuration particularly suited to the transmission of data over SSB mobile ratio networks," *IEEE Trans. Commun.*, vol. COM-32, pp. 81–87, Jan. 1984.

[12] M. K. Simon, "Dual-pilot tone calibration technique," *IEEE Trans. Veh. Technol.*, vol. VT-35, pp. 63–70, May 1986.

[13] P. M. Martin, A. Bateman, J. P. McGeehan, and J. D. Marvill, "The implementation of a 16-QAM mobile data system using TTIB-based fading correction techniques," in *IEEE VTC'88*, June 1988, pp. 71–76.

[14] F. Davarian, "Mobile digital communications via tone calibration," *IEEE Trans. Veh. Technol.*, vol. VT-36, pp. 55–62, May 1987.

[15] I. Korn, "Coherent detection of M-ary phase-shift keying in the satellite mobile channel with tone calibration," *IEEE Trans. Commun.*, vol. 37, pp. 997–1003, Oct. 1989.

[16] J. K. Cavers, "Performance of tone calibration with frequency offset and imperfect pilot filter," *IEEE Trans. Veh. Technol.*, vol. 40, pp. 426–434, May 1991.

[17] J. P. A. Albuquerque and P. H. G. Coelho, "On the performance of pilot-aided coherent detection of M-ary PSK carriers in mobile satellite communications," *IEEE Trans. Veh. Technol.*, vol. 43, pp. 597–603, Aug. 1994.

[18] M. F. Tariq, A. R. Nix, and D. Love, "Efficient implementation of pilot-aided 32 QAM for fixed wireless and mobile ISDN application," in *Proc. IEEE VTC'00*, May 2000, pp. 680–684.

[19] M. L. Moher and J. H. Lodge, "TCMP—A modulation and coding strategy for Rician fading channels," *IEEE J. Select. Areas Commun.*, vol. 7, pp. 1347–1355, Dec. 1989.

[20] J. K. Cavers, "An analysis of pilot symbol assisted modulation for Rayleigh-fading channels," *IEEE Trans. Veh. Technol.*, vol. 40, pp. 686–693, Nov. 1991.

[21] M. Li, "Narrow band mobile data communication using channel sounding techniques," Ph.D. dissertation, Dept. Elect. Electron. Eng., Univ. Bristol, Bristol, U.K., 1991.

[22] S. Sampei and T. Sunaga, "Rayleigh fading compensation for QAM in land mobile radio communications," *IEEE Trans. Veh. Technol.*, vol. 42, pp. 137–147, May 1993.

[23] Y. S. Kim, C. J. Kim, G. Y. Jeong, Y. J. Bang, H. K. Park, and S. S. Choi, "New Rayleigh fading channel estimator based on PSAM channel sounding technique," in *Proc. IEEE Int. Conf. Communications (ICC'97)*, June 1997, pp. 1518–1520.

[24] F. Adachi, M. Feeney, A. Williamson, and J. Parsons, "Crosscorrelation between the envelopes of 900 MHz signals received at a mobile radio base station site," *Proc. Inst. Elect. Eng.*, pt. F, pp. 506–512, Oct. 1986.

[25] A. M. D. Turkmani, A. A. Arowojolu, P. A. Jefford, and C. J. Kellett, "An experimental evaluation of the performance of two-branch space and polarization diversity schemes at 1800 MHz," *IEEE Trans. Veh. Technol.*, vol. 44, pp. 318–326, May 1995.

[26] S. Chennakeshu and J. B. Anderson, "Error rates for Rayleigh-fading multichannel reception of MPSK signals," *IEEE Trans. Commun.*, vol. 43, pp. 338–346, Feb./Mar./Apr. 1995.

[27] R. E. Ziemer and T. B. Welch, "Equal-gain combining of multichannel DPSK in Doppler-spread fading," *IEEE Trans. Veh. Technol.*, vol. 49, pp. 1846–1855, Sept. 2000.

[28] V. A. Aalo, "Performance of maximal-ratio diversity systems in a correlated Nakagami-fading environment," *IEEE Trans. Commun.*, vol. 43, pp. 2360–2369, Aug. 1995.

[29] P. Lombardo, G. Fedele, and M. M. Rao, "MRC performance for binary signals in Nakagami fading with general branch correlation," *IEEE Trans. Commun.*, vol. 47, pp. 44–52, Jan. 1999.

[30] L. Fang, G. Bi, and A. C. Kot, "New method of performance analysis for diversity reception correlated Rayleigh-fading signals," *IEEE Trans. Veh. Technol.*, vol. 49, pp. 1807–1812, Sept. 2000.

[31] J. Luo, J. R. Zeidler, and S. McLaughlin, "Performance analysis of compact antenna arrays with MRC in correlated Nakagami fading channels," *IEEE Trans. Veh. Technol.*, vol. 50, pp. 267–277, Jan. 2001.
[32] Q. T. Zhang, "Exact analysis of postdetection combining for DPSK and NFSK systems over arbitrarily correlated Nakagami channels," *IEEE Trans. Commun.*, vol. 46, pp. 1459–1467, Nov. 1998.
[33] P. Lombardo and G. Fedele, "Post-detection in Nakagami-fading channels with correlated branches," *IEEE Commun. Lett.*, vol. 3, pp. 132–135, May 1999.
[34] R. K. Mallik and M. Z. Win, "Error probability of binary NFSK and DPSK with postdetection combining over correlated Rician channels," *IEEE Trans. Commun.*, vol. 48, pp. 1975–1978, Dec. 2000.
[35] M.-S. Alouini and M. K. Simon, "Multichannel reception of digital signals over correlated Nakagami fading channels," in *Proc. 36th Allerton Conf. Communications Control Computing*, Sept. 1998, pp. 146–155.
[36] D. L. Noneaker and M. B. Pursley, "Error probability bounds for M-PSK and M-DPSK and selective fading diversity channels," *IEEE Trans. Veh. Technol.*, vol. 43, pp. 997–1004, Nov. 1994.
[37] J. R. Abeysinghe and J. A. Roberts, "Bit error rate performance of antenna diversity systems with channel correlation," in *Proc. IEEE GLOBECOM*, Nov. 1995, pp. 2022–2026.
[38] D. D. N. Bevan, V. T. Ermolayev, and A. G. Flaksman, "Coherent multichannel reception of binary modulated signals with dependent Rician fading," *Proc. Inst. Elect. Eng. Commun.*, vol. 148, pp. 105–111, Apr. 2001.
[39] E. Perahia and G. J. Pottie, "On diversity combining for correlated slowly flat-fading Rayleigh channels," in *Proc. IEEE ICC'94*, May 1994, pp. 342–346.
[40] Y. Cho and J. H. Lee, "Effect of fading correlation on the SER performance of M-ary PSK with maximal-ratio combining," *IEEE Commun. Lett.*, vol. 3, pp. 199–201, July 1999.
[41] P. Schramm and R. R. Muller, "Pilot symbol assisted BPSK on Rayleigh-fading channels with diversity: Performance analysis and parameter optimatization," *IEEE Trans. Commun.*, vol. 46, pp. 1560–1563, Dec. 1998.
[42] M. J. Barrett, "Error probability for optimal and suboptimal quadratic receivers in rapid Rayleigh fading channels," *IEEE J. Select. Areas Commun.*, vol. SAC-5, pp. 302–304, Feb. 1987.
[43] Y. C. Chow, J. P. McGeehan, and A. R. Nix, "Simplified error bound analysis for M-DPSK in fading channels with diversity reception," *Proc. Inst. Elect. Eng. Commun.*, vol. 141, pp. 341–350, Oct. 1994.

Yuk C. Chow (S'91–A'97) was born in Hong Kong, in 1969. He received the B.Eng. degree from the University of Glasgow, Glasgow, U.K., in 1990, the M.Sc. and D.I.C. degrees from Imperial College, University of London, London, U.K., in 1991, and the Ph.D. degree from the University of Bristol, Bristol, U.K., in 1997.

From 1995 to 1997, he was a Research Assistant in the Department of Electrical and Electronic Engineering, University of Bristol. He was with Motorola Semiconductors Hong Kong Ltd., from 1997 to 1999. He now is a Principal Research Engineer with Toshiba Research Europe Ltd., Bristol, U.K. His research interests include digital modulations, receiver-processing techniques, and transmitter/receiver system modeling.

Joe P. McGeehan received the B.Eng. and Ph.D. degrees in electrical and electronic engineering from the University of Liverpool, Liverpool, U.K., in 1967 and 1971, respectively.

He now is a Professor of Communications Engineering and Dean of the University of Bristol. He also is Managing Director of the Telecommunications Research Laboratory, Toshiba Research Europe Ltd., Bristol, U.K. He has been actively researching spectrum-efficient mobile radio communication systems since 1973 and has pioneered work in many areas, including linear modulation, linearized power amplifiers, smart antennas, propagation modeling/prediction using ray tracing, and phase-locked loops.

Dr. McGeehan is a Fellow of the Royal Academy of Engineering and of the Institution of Electrical Engineers (IEE), U.K. He has served on numerous international committees and standards bodies and was advisor to the U.K.'s first DTI/MOD "Defence Spectrum Review Committee" in the late 1970s. He was the Joint Recipient of the IEEE TRANSACTIONS ON VEHICULAR TECHNOLOGY Award—Neal Shepherd Memorial Award (for work on smart antennas) and of the IEE Proceedings Mountbatten Premium for work on satellite tracking and frequency-control systems.